Stimulated Brillouin scattering in silica optical nanofibers

Maxime Zerbib,[1] Moise Deroh,[2] Thibaut Sylvestre,[1] Kien Phan Huy,[1,3] and Jean-Charles Beugnot[1]
[1)]*Institut FEMTO-ST, Université de Franche-Comté, CNRS UMR 6174, Besançon, France*
[2)]*Laboratoire ICB, Université de Bourgogne, CNRS UMR 6303, Dijon, France*
[3)]*SUPMICROTECH-ENSMM, Besançon, France*

(*Electronic mail: maxime.zerbib@femto-st.fr)

(Dated: 25 September 2024)

Stimulated Brillouin scattering offers a broad range of applications, including lasers, sensors, and microwave photonics, most of which require strong Brillouin gain within a narrow bandwidth. Here, we experimentally report the first measurement of stimulated Brillouin scattering in silica optical nanofibers from both hybrid and surface acoustic waves. Using a pump-probe technique in the radio-frequency domain, we measured a Brillouin gain as high as 15 $m^{-1}W^{-1}$ and linewidth to 16 MHz for the L03 hybrid acoustic mode near 9 GHz using a 990-nm diameter nanofiber. This gain is 65 times larger than the highest gain obtained in standard single-mode fibers. Additionally, we report a Brillouin gain of up to 5 $m^{-1}W^{-1}$ from surface acoustic waves around 5 GHz. We further demonstrate a nanofiber-based Brillouin laser with a threshold of 350 mW. Our results create opportunities for advanced Brillouin-based applications utilizing optical nanofibers.

I. INTRODUCTION

Tapered optical nanofibers (ONFs) are of great interest in many areas of research, ranging from fundamental physics to practical applications, due to their unique mechanical, acoustic, and optical properties[1]. These highly tapered subwavelength waveguides provide a wide evanescent optical field, enabling a range of advanced applications, including quantum technologies[2], particle trapping[3], highly-sensitive optical sensing[4,5], high-resolution imaging[6], precise optical delay lines[7,8], and high Q factor micro-resonators[9,10]. Additionally, the tight transverse confinement of light within ONFs significantly enhances optical nonlinear processes, such as four-wave mixing (FWM)[11], stimulated Raman scattering (SRS)[12], supercontinuum generation (SCG)[13], and stimulated Brillouin scattering (SBS)[14–16]. SBS, in particular, is crucial in optical nanofibers as it promotes a variety of photon-phonon interactions, resulting in a multi-peak Brillouin spectrum[14]. Recently, stimulated intermodal Brillouin scattering process in a silica nanofiber demonstrates an efficiency of 300 $m^{-1}W^{-1}$ for an acoustic wave frequency of 204 MHz[17]. Unlike standard optical fibers, ONFs carry several acoustic waves, including surface acoustic waves (SAWs) and hybrid waves (HAWs), which combine longitudinal and transverse components, each generating its own distinct Brillouin resonance in a range from 5 GHz to 10 GHz[15]. However, to date, only spontaneous Brillouin scattering from these various acoustic waves has been evidenced, thereby limiting the potential applications.

In this paper, we report the observation of SBS from hybrid and surface acoustic waves in long, and ultra-low loss silica optical nanofibers. We adapt a pump-probe experiment in the radio-frequency (RF) domain to isolate and measure the backward Brillouin gain for these close acoustic resonances. Using this method, we quantify a Brillouin gain coefficient g_B=15$m^{-1}W^{-1}$ for the L03 hybrid wave, using a nanofiber with a diameter of 990 nm, a length of 180 mm, and total insertion losses as low as 0.2 dB. We also report peak gain values for TR21 and L01 Stokes signals backscattered from SAWs, at 5 $m^{-1}W^{-1}$ and 3.5 $m^{-1}W^{-1}$, respectively, using a shorter 100 mm-long nanofiber with a 740 nm diameter. These measurements align closely with theoretical predictions, accounting for the influence of nanofiber diameter variations. Based on these results, we set up a Brillouin ring cavity based on the 990-nm nanofiber and demonstrate a Brillouin laser effect with a threshold power of 385 mW, in quite good agreement with theoretical predictions.

The paper is divided into four sections. Section II details the experimental method for measuring Brillouin gain in the RF domain. Section III presents the experimental measurements of backward SBS gain in silica optical nanofibers for both hybrid and surface acoustic waves. In Section IV, we provide numerical gain calculations based on an electrostrictive model that accounts for diameter fluctuations along the nanofiber. Finally, in Section V, we describe the nanofiber-based Brillouin laser and show its performances.

II. EXPERIMENTAL METHOD AND SETUP

The Brillouin gain of an optical waveguide is commonly assessed by determining the g_B small coefficient, expressed in $m^{-1}W^{-1}$. Several methods exist to measure this gain. One common optical method, based on a pump-probe technique, involves detecting the amplification of the probe wave when a continuous pump wave. with increasing power, is injected in the opposite direction[18]. This method is widely used for its accuracy and ease of application, providing a direct measure of the gain in dB and subsequently in then $m^{-1}W^{-1}$. However, this approach is not well suited for determining the Brillouin gain in optical nanofibers (ONFs), as these exhibit many acoustic waves. Coupled with the high thermal sensitivity of ONFs, this measurement would require tunable narrow filters to discriminate the contribution of each signal to the total backscattered power. To address similar challenges in photonic integrated circuits (PICs), new RF methods for g_B evaluation from the radio-frequency (RF) domain have recently been established[19,20]. Among these, accurate gain measure-

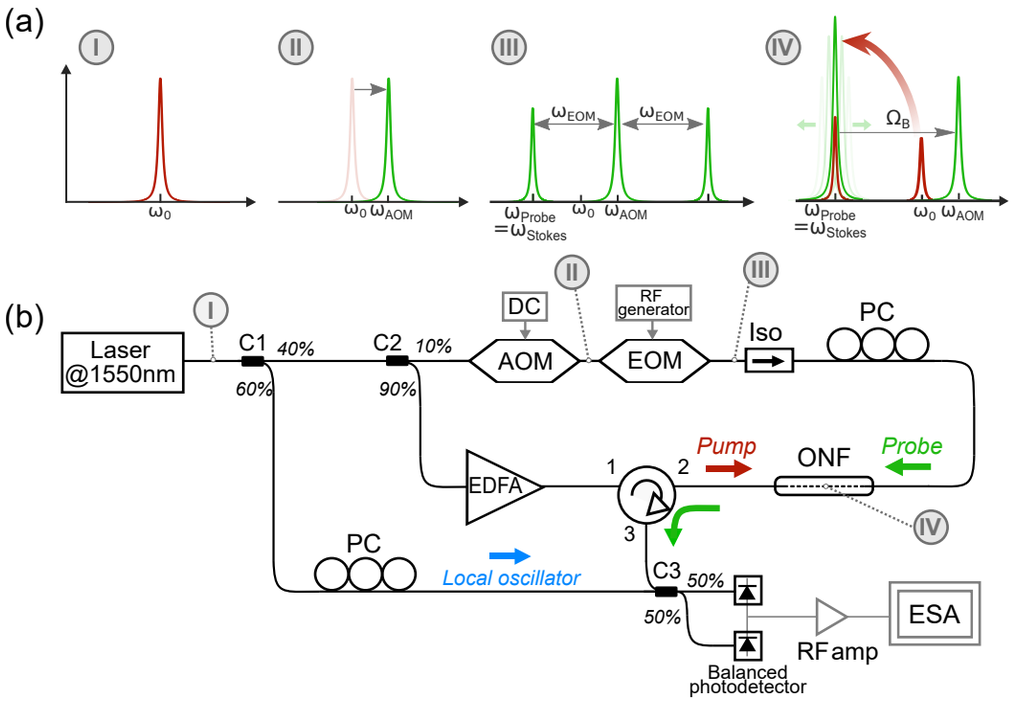

FIG. 1. **Brillouin gain measurement in silica optical nanofibers using a pump-probe configuration.** **(a)** Schemes of the various steps involved in shaping the probe and pump frequencies (I-IV). **I** Laser center frequency ω_0. **II** Laser frequency shifting at $\omega_{AOM} = \omega_0 + 80MHz$ using an acousto-optic modulator (AOM). **III** Sidebands generation at $\omega_{AOM} \pm \omega_{EOM}$ using an electro-optic modulator (EOM). **IV** Probe amplification by Brillouin scattering. Probe frequency ω_{probe} coincides with the nanofiber Brillouin Stokes frequency $\omega_{Stokes} = \omega_0 - \omega_B$, where ω_B is the acoustic frequency. Subject to polarization-matching, the pump energy is transferred to the probe as ω_{probe} scans the Stokes resonance. **(b)** Experimental SBS set-up based on heterodyne detection. C1,2,3: directional couplers, AOM: Acousto-optic modulator, EOM: Electro-optic modulator, Iso: Isolator, PC: Polarization controllers, EDFA: Erbium-Doped Fiber Amplifier, ONF: Optical nanofiber, RF Amp: radio-frequency amplifier, ESA: Electrical spectrum analyzer. Note that RBW = 2 MHz and VBW = 20 kHz.

ment has been demonstrated in the RF domain using a vector network analyzer (VNA)[20].

In our study, we used heterodyne detection on electrical domain for Brillouin gain measurement. Additionally, our procedure ensures the small Brillouin gain approximation, maintaining low optical probe power, and facilitating measurements within the non-depleted stimulated regime.

The experimental setup is depicted in Fig. 1. As a pump laser, we use a 1550-nm narrow-linewidth continuous-wave (CW) distributed-feedback fiber laser at frequency denoted ω_0 (step I)/ This laser is then split into two channels using a fiber coupler (C1). The lower channel is used as a local oscillator (LO), while the upper is used for the probe and the pump using a second coupler (C2). The lower path after C2, which serves as the Brillouin pump, is amplified with an Erbium-doped fiber amplifier (EDFA) up to P_P = 23.4 dBm. This pump is then transmitted to the nanofiber through an optical circulator, triggering spontaneous Brillouin backscattering at frequency ω_{Stokes}. The upper path of C2 is used to shape the probe signal. An acousto-optic modulator (AOM) first shifts the probe frequency to $\omega_{AOM} = \omega_0 + 80$ MHz (step II). An electro-optic modulator (EOM) then generates small sidebands at frequencies $\omega_{AOM} \pm \omega_{EOM}$ (step III). As a result, after passing through an isolator (ISO) and a polarization controller (PC), the probe enters the ONF in the counter-propagating direction with a frequency $\omega_{probe} = \omega_{Stokes} = \omega_{AOM} - \omega_{EOM}$. When polarization is well aligned, the pump energy is transferred to the probe as the Stokes frequency is swept by the RF generator (step IV). Using the AOM offers dual advantages. First, it triggers the Stokes process without stimulating the anti-Stokes process. Second, it allows us to remove all parasitic non-optical signals from the RF generator, which could otherwise interfere with the measurements and be detected by the fast photodiode.

After the Brillouin interaction, the amplified probe is directed through circulator port 2 to port 3, where it is combined with the LO using a third coupler (C3). A polarization controller (PC) is introduced in the LO path to optimize RF beat signal onto the photo-detector. We use a fast balanced photodetector (Bandwidth equal to 43 GHz) to improve the RF signal, which is further amplified using an RF amplifier and finally detected using an electrical spectrum analyzer (ESA). Direct measurement of probe amplification through Brillouin scattering is performed from the ESA. In this setup, maintaining the optical power of the probe close to that of a spontaneously backscattered Stokes signal (typically -40 dBm) is crucial. This not only prevents detector saturation but also ensures reliable probe linear amplification measurement on the

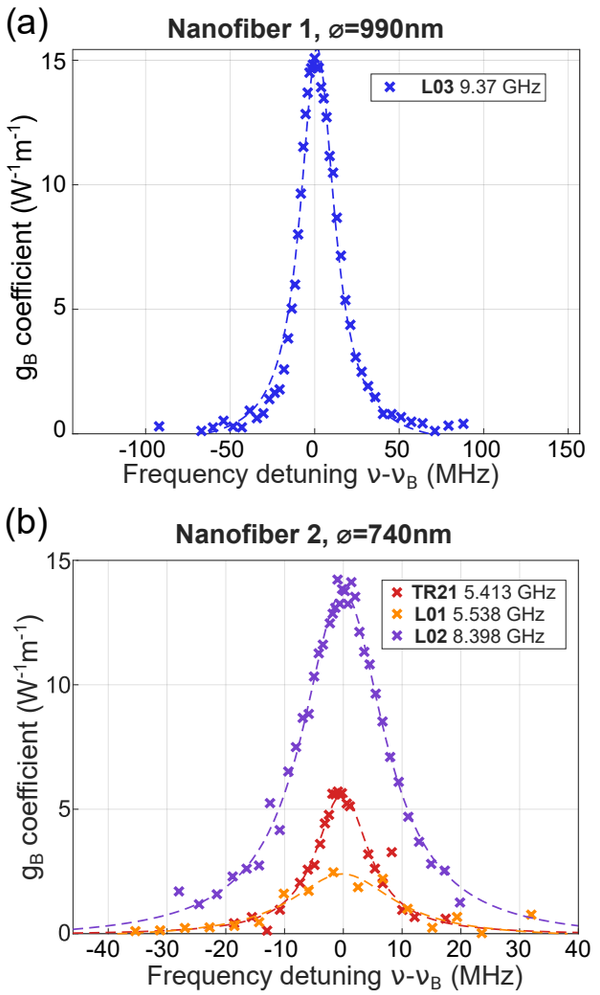

FIG. 2. **Experimental Brillouin gain spectra for two silica nanofibers.** (a) Nanofiber 1: $L = 180$ mm, $\Phi = 990$ nm. The observed Stokes resonance is associated with the L03 acoustic wave at $\nu_B = 9.37$ GHz. The experimental data are depicted by blue crosses and fitted with a Lorentzian curve shown as a blue dashed curve. (b) Nanofiber 2: $L = 100$ mm, $\Phi = 740$ nm. The Brillouin gain response exhibits multiple frequencies corresponding to the acoustic resonances L02 (purple), L01 (orange), and TR21 (red) and fitted with a Lorentzian curve in dashed curve.

ESA. Achieving this balance involves managing the frequency resolution and noise averaging over a given bandwidth, controlled respectively by the ESA resolution bandwidth (RBW) and video bandwidth (VBW) parameters. The peak detected on the ESA represents the optical beat intensity resulting from the interference between the probe wave and the local oscillator. This is then converted into the RF domain using a broadband photodiode. A band power integration around the probe peak center frequency yields the RF power, which is proportional to the optical power of the probe[21]. By comparing probe RF power measurements with and without interaction (pump ON/OFF) while sweeping its frequency, we determine the probe amplification and calculate the Brillouin gain coefficient, applying the following equation

$$g_B = \ln\left(\frac{P_S}{P_S^0}\right)\frac{1}{P_P L_{eff}}, \tag{1}$$

where g_B is the Brillouin gain coefficient in $m^{-1}W^{-1}$, P_S and P_S^0 are the RF probe powers in W, with and without Brillouin gain (pump ON/OFF), respectively, P_P is the optical pump power (W) and L_{eff} is the effective length (m). Further details about the method can be found in the Appendix I. It not only makes it possible to measure the Brillouin efficiency when the optical power of the backscattered signal is low, but also offers the advantage of finely scanning a bandwidth with the probe. This method allow measuring a very low Brillouin gain because the very low loss on nanofiber induce a very low pump reflection.

III. EXPERIMENTAL RESULTS

The ONFs were fabricated by heating and tapering uncoated standard single-mode fibers (SMFs) using the heat-brush technique[15,22]. This technique is mainly based on the use of a butane flame and two motorized translation stages to heat and taper the fiber. The nanofiber length and taper transition shapes were meticulously controlled by the computed trajectories of two translation stages, while the butane flame remained motionless. Employing this technique, we achieved fiber waists as narrow as 740 nm over a uniform length of up to 180 mm. The transition regions were adiabatically drawn to ensure single-mode conversion from the SMF to the nanofiber, achieving low insertion loss down to 0.2 dB at 1550 nm.

Our initial investigation focused on a nanofiber with a diameter of 990 nm and a uniform length of 180 mm, chosen for its ability to maximize the opto-acoustic coupling due to its minimal effective mode area[23]. The experimental Brillouin gain spectrum is represented by blue crosses in Fig.2(a). A Brillouin peak gain of $g_B = 15\,m^{-1}W^{-1}$ is achieved at a probe frequency of $\nu_B = 9.37$ GHz (Nanofiber 1). In contrast, the measurement performed using a single-mode fiber (SMF-28) at a center frequency of 10.81 GHz results in a significantly lower gain $g_B = 0.23\,m^{-1}W^{-1}$. The nanofiber's gain was approximately 65 times higher than that of the SMF-28 at 1550 nm [18]. A Lorentzian fit of the gain spectrum (denoted by the blue dashed line) indicates a full-width at half-maximum (FWHM) of 24 MHz. In Fig. 2(b), we present measurements of the Brillouin gain spectra for three acoustic waves using another 100 mm-long nanofiber with a smaller 740 nm waist diameter (Nanofiber 2). This fiber diameter was determined from numerical simulations to get the maximum SBS gain for surface acoustic waves[14,16]. This will be detailed in the next section. The three acoustic resonances shown in Fig. 2(b) include the hybrid acoustic wave L02 and the surface acoustic waves (SAWs) L01 and TR21, whose frequencies are indicated in the inset of Fig. 2(b). The L02 resonance of Nanofiber 2 (depicted in purple) has a center frequency of

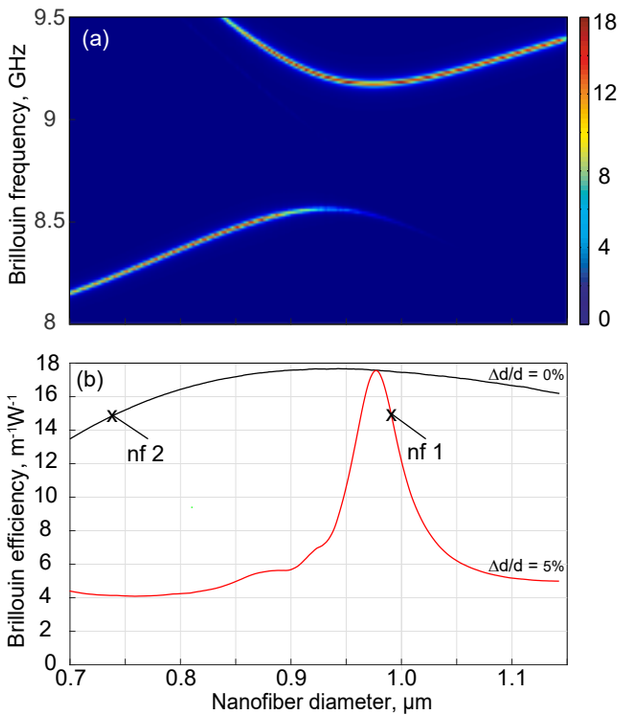

FIG. 3. **Numerical Brillouin gain in optical nanofibers**. (a) Numerical 3D Brillouin gain spectra in silica nanofiber for a diameter ranging from 0.7 μm to 1.15 μm showing two hybrid acoustic waves. (b), Numerical calculation of Brillouin gain as a function of diameter in silica nanofiber. The impact of a 5% linear fluctuation in diameter along the nanofiber is represented in red. The experimental Brillouin gains in nanofibers (nf1 and nf2) are represented by the circle point.

8.4 GHz and a linewidth of 17 MHz, demonstrating a similar gain value (g_B = 14.5 $m^{-1}W^{-1}$), as the one of Nanofiber 1 at 9.37 GHz. Despite the lower opto-acoustic overlap, we also observe a strong intrinsic Brillouin gain of 3.5 $m^{-1}W^{-1}$ and 5 $m^{-1}W^{-1}$ for surface acoustic waves, L01 and TR21, at frequencies of 5.538 GHz and 5.413 GHz, respectively. This is quite impressive because the opto-acoustic transverse overlap is very weak as it primarily relies on the optical evanescent field. The effective area of nf1 and nf2 are equal to 1.47 μm^2 and 2.17 μm^2, respectively. Note that the presence of multiple Brillouin gain resonances as those observed here can be advantageous for microwave photonics applications[24,25].

IV. NUMERICAL MODELING

To estimate the Brillouin gain and identify the optimal nanofiber diameters, we solve the elastodynamics equation driven by the electrostrictive stress governing Brillouin photon-phonon scattering[26]. In nanofibers with subwavelength diameters, strong phonon dispersion induces a nonlinear variation of Brillouin resonances as a function of core diameter, resulting in various longitudinal, surface, and hybrid acoustic waves[14,27,28]. Figures 3(a) and (b) illustrate this phonon dispersion and the Brillouin gain efficiency for fiber diameters ranging from 0.7 μm to 1.15 μm, respectively. Figure 3(b) also indicates the nanofiber diameter that provides the highest Brillouin gain for hybrid acoustic waves, which is directly related to the transverse spatial distribution of the fundamental optical mode. The optimal diameter, shown by the black curve, is 940 nm, corresponding to maximum light and sound confinement for a pump wavelength of 1550 nm.

The Brillouin gain lineshape is directly influenced by nanofiber diameter variations. These variations, caused by the tapering process, are the main source of optical losses[29]. Figure 3(b) shows that, for diameters ranging from 830 nm to 1060 nm, the Brillouin gain exceeds 17 $m^{-1}W^{-1}$ (black line). To assess the impact of fiber non-uniformity, we calculated the Brillouin gain for linear diameter fluctuations of 5%. The result, shown in Fig. 3(b), is depicted in red. For diameters around 980 nm $\pm$ 10 nm, the Brillouin gain remains relatively unaffected by these fluctuations, as shown in Fig. 3(a). At this diameter, strong coupling of the axial shear and axial longitudinal elastic components induces a curvature in the phase-matching condition, and the Brillouin resonance of the L03 mode remains constant for an ONF diameter ranging from 950 nm to 1.0 μm. Consequently, a Brillouin gain greater than 15 $W^{-1}m^{-1}$ can be achieved with 5% diameter fluctuations along the nanofiber, for a diameter of 975 nm $\pm$ 25 nm. The numerically predicted Brillouin gains are in very good agreement with the experimentally reported results for hybrid acoustic waves, as shown in Fig. 2. Specifically, Nanofiber 2 (nf2) exhibits a diameter variation of less than 1%, achieving a maximum Brillouin gain of 15 $W^{-1}m^{-1}$ for a diameter of 740 nm. For Nanofiber 1 (nf1), there is good agreement between the measured Brillouin gain and theoretical predictions for a diameter fluctuation of 5%. These diameter fluctuations are attributed to the extended length of the nanofiber, which at 180 mm represents the maximum length achieved using the heat-brush tapering technique.

V. NANOFIBER-BASED BRILLOUIN LASER

Brillouin lasers have been extensively studied in the past due to their unique characteristics, including highly coherent, ultra-narrow linewidth emission. These properties make them particularly suitable for applications such as laser linewidth narrowing and microwave generation[30,31]. A variety of Brillouin lasers have been demonstrated using single-mode silica fibers, chalcogenide tapers, and even more recently photonic integrated circuits[30–32]. We can leverage the large Brillouin gain in silica nanofibers to build such a Brillouin laser. For this purpose, we use nanofiber 2 (nf2) due to its long length and high gain efficiency ($\Phi = 990$ nm, $L = 180$ mm). Figure 4(a) shows the experimental setup of the Brillouin laser cavity under non-resonant pumping conditions. The initial narrow-linewidth pump fiber laser is split into two parts using a tap coupler (C1). The first part is polarization controlled (PC), subsequently amplified, and used as the pump for SBS. The

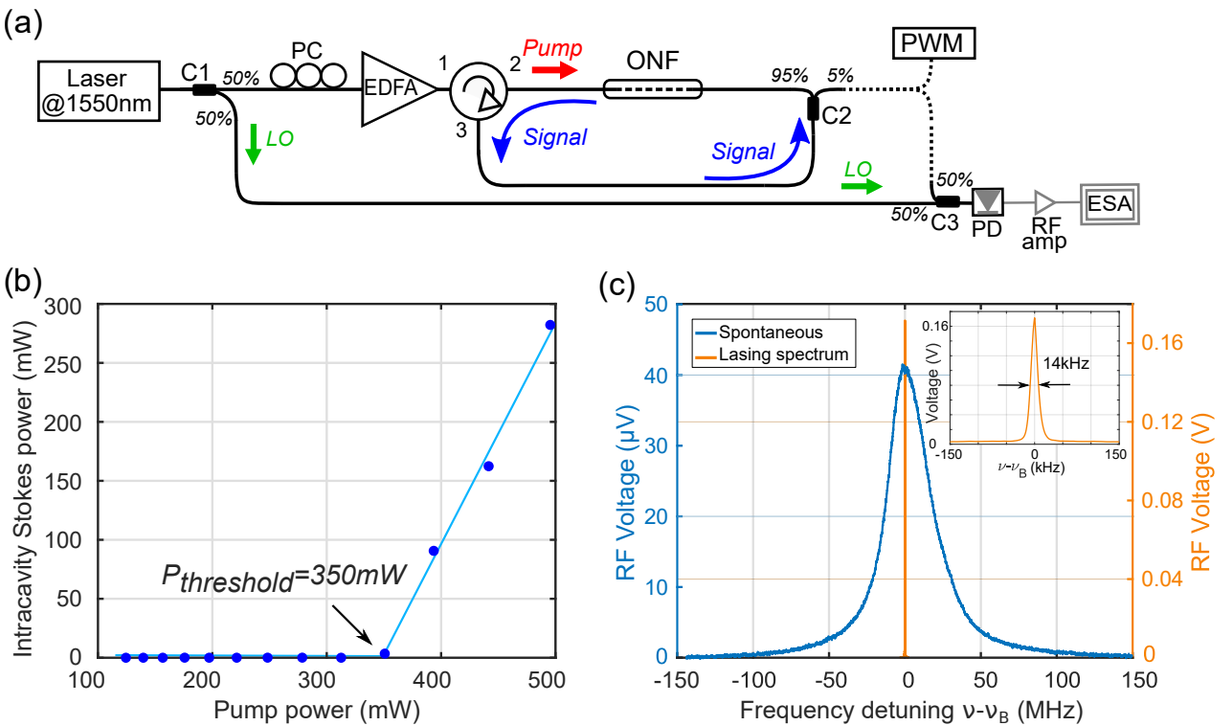

FIG. 4. **Nanofiber-based Brillouin laser (a)** Scheme of the experimental setup of the non-reciprocal fiber ring cavity including the optical nanofiber (ONF). The cavity end is connected to an optical power-meter (PWM) for laser threshold measurement or mixed with a local oscillator for laser linewidth characterization in the electrical domain. C1,2,3: directional couplers, PC: polarization controllers, EDFA: Erbium-Doped Fiber Amplifier, PD: photodiode, RF Amp: RF amplifier, ESA: Electrical spectrum analyzer. **b** Intracavity Brillouin Stokes power as a function of the input pump power. A power threshold is reached at $P_{threshold} = 350\,\mathrm{mW}$ **(c)** Spontaneous Brillouin (blue) and laser (orange) spectra. The inset shows a zoom on the laser spectrum, revealing narrowing linewidth as compared to spontaneous Brillouin spectrum.

pump beam then enters the loop-shaped fiber cavity through an optical circulator, where it propagates within the nanofiber and generates a backward Brillouin signal, with a frequency offset of $\nu_B = 9.37\,\mathrm{GHz}$ from the pump. The signal is directed from circulator port 2 to port 3 and travels to the 95/5 tap coupler C2, where 95% of the signal is fed back into the cavity. The remaining 5% is split into two paths: one part is sent to an optical power meter (PWM) for lasing threshold characterization, and the other part is used to create the beat note signal with the initial laser to measure the laser linewidth. In this ring fiber cavity configuration, only the Stokes signal resonates, while the pump signal is isolated by the optical circulator. The total cavity losses are 2.8 dB, primarily attributed to the circulator (1 dB) and the coupler (1.5 dB), with the ONF contributing only 0.3 dB. The total cavity length is 4.05 m including SMF pigtails and the nanofiber. In this configuration, the free spectral range of the cavity is equal to 51 MHz and only one cavity mode oscillate below the Brillouin gain curve, enabling single-frequency lasing.

We have thoroughly checked that the laser does not resonate at the single-mode fiber (SMF) Brillouin frequency (10.86 GHz).

The Brillouin Stokes power inside the cavity as a function of the injected pump power is shown in Fig. 4(b). At a pump power of $P_p = 350\,\mathrm{mW}$, a threshold appears, and the Stokes power in the cavity increases linearly with a steep slope, confirming the Brillouin laser effect beyond this limit. A laser power of 280 mW is obtained for a pump power of 500 mW. This experimental threshold value is in good agreement with the theoretical Brillouin threshold of 348 mW, detailed in the Appendix II. The conversion rate above the laser threshold is about 50%. Each optical power measurement is averaged over several counts to account for the thermal drift of the nanofiber ring cavity relative to the pump laser. In this configuration, the stability of the laser is not optimized.

Next, we measured the Brillouin laser linewidth around the nanofiber's L03 frequency at 9.37 GHz based on the heterodyne detection and using the ESA. Figure 4(c) shows both the laser beat note spectrum in orange and for comparison the spontaneous Brillouin spectrum in blue. The upper-right inset provides a closer form of the lasing spectrum, displaying a clear demonstration of gain regimes.

VI. CONCLUSION AND OUTLOOKS

To summarize, in this work, we experimentally demonstrated backward Brillouin amplification in silica optical nanofibers, both from hybrid and surface acoustic waves. A Brillouin gain of $15\,\mathrm{W^{-1}m^{-1}}$ was achieved for hybrid waves using a 180 mm long nanofiber with a diameter of 990 nm, while a gain of $5\,\mathrm{W^{-1}m^{-1}}$ was measured for surface acoustic waves using a 100 mm long nanofiber with a diameter of 740 nm. For these measurements, we developed an innovative pump-probe technique in the RF domain, which notably does not require optical or RF filters, enabling accurate gain measurement of spectrally close resonances. Our gain measurements were accurately predicted by numerical calculations of the Brillouin gain based on the elastodynamics equation and taking into account the impact of diameter fluctuations along the nanofiber. We identified a nanofiber diameter for which geometric variations (up to 5%) did not impact the Brillouin gain linewidth. These specific diameters for Brillouin interactions serve as a source of high gain for nonlinear conversion.

Furthermore, stimulated Brillouin scattering in nanofibers was applied to demonstrate a Brillouin laser based on a 180 mm-long low-loss nanofiber with a diameter of 990 nm, achieving a threshold of 350 mW. This nanofiber-based Brillouin laser holds promise as a low-noise reference laser source. A future step involves implementing a phase-locking loop system to stabilize the beat note signal to an external oscillator[33,34]. This will effectively suppress any thermal drift of the ONF cavity relative to the pump laser, considering our system lacks thermal isolation. Compared to other fiber systems, low-loss ONFs significantly reduce the interaction length required to achieve the Brillouin laser effect, providing a more efficient and compact solution. Additionally, the capability to transmit high continuous-wave power in nanofibers[13] opens avenues for applications of SBS in all-fiber microwave photonics and coherent lasers.

APPENDIX I: METHOD FOR BRILLOUIN GAIN MEASUREMENT

The Brillouin efficiency coefficient is measured by heterodyning the probe in RF domain and by using the well-known formula:

$$P_S = P_S^0 \exp^{g_B P_P L_{eff}} \tag{2}$$

where $P_S = P_S(L)$ and $P_S^0 = P_S(0)$ are respectively the detected optical probe powers in W, with and without SBS interaction in the ONF (pump ON/OFF), g_B is the Brillouin gain coefficient ($W^{-1}m^{-1}$), P_P, the optical pump power (W) and L_{eff}, the effective length (m). Equation 2 can be written as:

$$g_B = \ln\left(\frac{P_S}{P_S^0}\right)\frac{1}{P_P L_{eff}} \tag{3}$$

The probe signal reaches the nanofiber with a low power ($> -40\,\mathrm{dBm}$) comparable to the power of a spontaneously backscattered signal. After interaction with the local oscillator, the beat frequency is detected on the spectrum analyzer. From a bandpower measurement around the probe resonance, we obtain an integrated value of the radiofrequency power (Fig. 5).

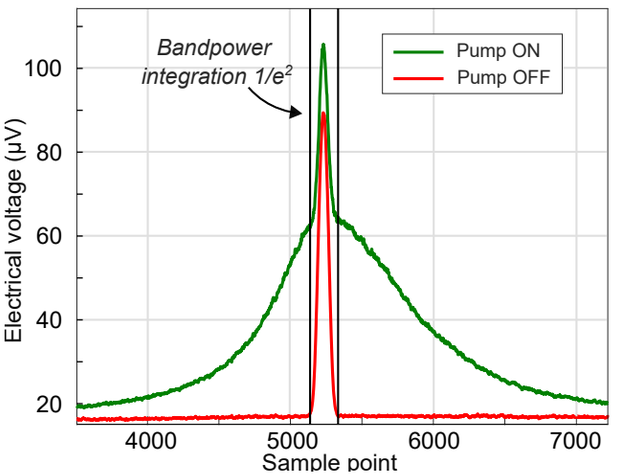

FIG. 5. Probe amplification measurement

At constant optical pump power, the ratio P_S/P_S^0 is equivalent to the RF powers ratio[21]:

$$\left[\frac{P_S}{P_S^0}\right]^{Opt} = \left[\frac{P_S}{P_S^0}\right]^{RF} \tag{4}$$

By taking measurements at constant pump power (ON/OFF) while scanning the probe frequency around the Brillouin resonance, we obtain a ratio value that can be injected into Equation 3.

APPENDIX II: BRILLOUIN LASER THRESHOLD

The Brillouin laser threshold of silica-based nanofiber cavity can be numerically calculated by solving the following coupled equations[35]. At each ONF cavity roundtrip, the stimulated Brillouin scattering process is computed under steady-state conditions.

$$\frac{d|A_P|^2}{dz} = \left(-\frac{\mathrm{Re}\left[g_B(\delta\Omega)\right]}{A_{eff}}|\tilde{A_S}|^2 - \alpha\right)|A_P|^2 \tag{5}$$

$$-\frac{d|\tilde{A_S}|^2}{dz} = \left(\frac{\mathrm{Re}\left[g_B(\delta\Omega)\right]}{A_{eff}}|A_P|^2 - \alpha\right)|\tilde{A_S}|^2 \tag{6}$$

$$|A_P(L)|^2 = P_{\mathrm{in}}^p \quad \text{and} \quad \tilde{A_S}^{(n)}(0) = \tilde{A_S}^{(n-1)}(L) \tag{7}$$

$$g_B(\delta\Omega) = \frac{g_B^0}{1 + 2i\,\delta\Omega/\Gamma_B}, \tag{8}$$

$$R = R_0 - (1 - 10^{(-\frac{\eta}{10})}), \tag{9}$$

$$F = \frac{\pi\sqrt{R}}{1-R}, \tag{10}$$

where $|A_P|^2$ and $|\tilde{A_S}|^2$ are the corresponding pump and Stokes powers. α is the attenuation coefficient of the ONF fiber and is neglected compared to the discrete cavity losses η (optical circulator, coupler, splices, etc.), which is related to both the cavity feedback parameter (R) and the spectral finesse (F) of the ONF ring cavity[36]. In our case, these parameters are estimated to be 45.7 % and 3.91, respectively. g_B^0 (in $W^{-1}.m^{-1}$) is the Brillouin gain efficiency, Γ_B (in MHz) is the Brillouin gain bandwidth, while $\delta\Omega$ (in MHz) is the mismatch between the Brillouin gain peak and the nearest lasing cavity mode, which can be finely controlled by tuning the pump laser frequency. We solve this step numerically using a boundary value problem solver[37] initialized with an analytical expression that assumes pump non-depletion[38]. This provides the spatial distribution of the pump power $A_P(z)$. Finally, the out-coupling (ratio $\theta = 5\%$ in our case) and total cavity losses η are applied to iterate from each roundtrip to achieve Stokes lasing operation. More details of the numerical model are given in Ref[39]. Here, the theoretical Brillouin lasing threshold is calculated to be 358 mW. This value mainly depends on the Brillouin gain efficiency in the fiber cavity and the total roundtrip losses, which are the most critical parameters. Optimizing cavity losses by splicing all the optical components including the optical circulator and the fiber coupler could significantly lower the lasing threshold. Underline that other simulation techniques are available to compute the dynamical response of the Brillouin lasing[40,41]. While these methods may be useful for modeling Brillouin gain competition and multimode Brillouin operation. The silica-based ONF cavity parameters used in our simulation are summarized in table I above.

ONF cavity parameters	Units	Value
Total roundtrip losses, η	dB	2.95
ONF length, L_{ONF}	m	0.18
Residual SMF-28 length, L_{SMF}	m	3.87
Total cavity length, L_{tot}	m	4.05
SBS frequency shift, ν_B	GHz	9.37
Brillouin gain efficiency, g_B/A_{eff}	$W^{-1}.m^{-1}$	15
Free spectral range, FSR	MHz	51.8
out-coupling, θ	%	5

TABLE I. Nanofiber cavity parameters used for Brillouin lasing threshold modeling. All parameters are measured except free spectral range

FUNDING

This work has been supported by the EIPHI Graduate school (contract ANR-17-EURE-0002) and by the Bourgogne Franche-Comté region.

DATA AVAILABILITY STATEMENT

Data underlying the results presented in this paper are not publicly available at this time, but may be obtained from the authors upon reasonable request

REFERENCES

[1]L. Zhang, Y. Tang, and L. Tong, "Micro-/nanofiber optics: Merging photonics and material science on nanoscale for advanced sensing technology," Iscience **23** (2020), 10.1016/j.isci.2019.100810.
[2]P. Solano, J. A. Grover, J. E. Hoffman, S. Ravets, F. K. Fatemi, L. A. Orozco, and S. L. Rolston, "Optical nanofibers: a new platform for quantum optics," in *Advances In Atomic, Molecular, and Optical Physics*, Vol. 66 (Elsevier, 2017) pp. 439–505.
[3]P. P. Kamath, S. Sil, V. G. Truong, and S. N. Chormaic, "Particle trapping with optical nanofibers: a review," Biomedical Optics Express **14**, 6172–6189 (2023).
[4]A. Godet, J. Chretien, K. P. Huy, and J.-C. Beugnot, "Micronewton nanofiber force sensor using Brillouin scattering," Optics Express **30**, 815–824 (2022).
[5]J. Yang, T. Qin, F. Zhang, X. Chen, X. Jiang, and W. Wan, "Multiphysical sensing of light, sound and microwave in a microcavity Brillouin laser," Nanophotonics **9**, 2915–2925 (2020).
[6]J. Sun, S.-J. Tang, J.-W. Meng, and C. Li, "Whispering-gallery optical microprobe for photoacoustic imaging," Photonics Research **11**, A65–A71 (2023).
[7]A. Matic, J. Chrétien, A. Godet, K. P. Huy, and J.-C. Beugnot, "Optical nanofiber stretcher," Optics Letters **48**, 3319–3322 (2023).
[8]M. Rezaei, G. T. Zeweldi, M. H. M. Shamim, and M. Rochette, "Single-mode optical fiber couplers made of fluoride glass," Opt. Express **31**, 27183–27191 (2023).
[9]M. Cai, O. Painter, and K. J. Vahala, "Observation of critical coupling in a fiber taper to a silica-microsphere whispering-gallery mode system," Physical Review Letters **85**, 74 (2000).
[10]M. Sumetsky, Y. Dulashko, J. Fini, A. Hale, and D. DiGiovanni, "The microfiber loop resonator: theory, experiment, and application," Journal of Lightwave Technology **24**, 242–250 (2006).
[11]M. I. A. Khudus, F. De Lucia, C. Corbari, T. Lee, P. Horak, P. Sazio, and G. Brambilla, "Phase matched parametric amplification via four-wave mixing in optical microfibers," Optics Letters **41**, 761–764 (2016).
[12]L. Shan, G. Pauliat, G. Vienne, L. Tong, and S. Lebrun, "Stimulated Raman scattering in the evanescent field of liquid immersed tapered nanofibers," Applied Physics Letters **102**, 201110 (2013).
[13]J. Zhang, Y. Kang, X. Guo, Y. Li, K. Liu, Y. Xie, H. Wu, D. Cai, J. Gong, Z. Shi, *et al.*, "High-power continuous-wave optical waveguiding in a silica micro/nanofibre," Light: Science & Applications **12**, 89 (2023).
[14]J.-C. Beugnot, S. Lebrun, G. Pauliat, H. Maillotte, V. Laude, and T. Sylvestre, "Brillouin light scattering from surface acoustic waves in a subwavelength-diameter optical fibre," Nature Communications **5** (2014), 10.1038/ncomms6242.
[15]A. Godet, A. Ndao, T. Sylvestre, V. Pecheur, S. Lebrun, G. Pauliat, J.-C. Beugnot, and K. P. Huy, "Brillouin spectroscopy of optical microfibers and nanofibers," Optica **4**, 1232–1238 (2017).
[16]O. Florez, P. F. Jarschel, Y. a. V. Espinel, C. M. B. Cordeiro, T. P. Mayer Alegre, G. S. Wiederhecker, and P. Dainese, "Brillouin scattering self-cancellation," Nature Communications **7**, 11759 (2016).
[17]W. Xu, M. Zerbib, A. Iyer, J.-C. Beugnot, and W. H. Renninger, "Ultranarrow-linewidth stimulated intermodal forward brillouin scattering," in *CLEO: Fundamental Science* (Optica Publishing Group, 2023) pp. FTh3B–3.
[18]M. Deroh, J.-C. Beugnot, K. Hammani, C. Finot, J. Fatome, F. Smektala, H. Maillotte, T. Sylvestre, and B. Kibler, "Comparative analysis of stimulated Brillouin scattering at 2µm in various infrared glass-based optical fibers," J. Opt. Soc. Am. B **37**, 3792–3800 (2020).
[19]R. Botter, K. Ye, Y. Klaver, R. Suryadharma, O. Daulay, G. Liu, J. van den Hoogen, L. Kanger, P. van der Slot, E. Klein, *et al.*, "Guided-acoustic stimulated Brillouin scattering in silicon nitride photonic circuits," Science advances **8**, eabq2196 (2022).

[20]K. Ye, Y. Klaver, O. A. Jimenez Gordillo, R. Botter, O. Daulay, F. Morichetti, A. Melloni, and D. Marpaung, "Brillouin and Kerr nonlinearities of a low-index silicon oxynitride platform," APL Photonics **8**, 051302 (2023).
[21]E. A. Kittlaus, H. Shin, and P. T. Rakich, "Large Brillouin amplification in silicon," Nature Photonics **10**, 463–467 (2016).
[22]T. A. Birks and Y. W. Li, "The shape of fiber tapers," Journal of Lightwave Technology **10**, 432–438 (1992).
[23]L. Tong, R. R. Gattass, J. B. Ashcom, S. He, J. Lou, M. Shen, I. Maxwell, and E. Mazur, "Subwavelength-diameter silica wires for low-loss optical wave guiding," Nature **426**, 816–819 (2003).
[24]W. Zhang and R. A. Minasian, "Switchable and tunable microwave photonic Brillouin-based filter," IEEE Photonics Journal **4**, 1443–1455 (2012).
[25]R. Pant, D. Marpaung, I. V. Kabakova, B. Morrison, C. G. Poulton, and B. J. Eggleton, "On-chip stimulated Brillouin scattering for microwave signal processing and generation," Laser & Photonics Reviews **8**, 653–666 (2014).
[26]J.-C. Beugnot and V. Laude, "Electrostriction and guidance of acoustic phonons in optical fibers," Physical Review B **86**, 224304 (2012).
[27]G. Neijts, C. K. Lai, M. K. Riseng, D.-Y. Choi, K. Yan, D. Marpaung, S. J. Madden, B. J. Eggleton, and M. Merklein, "On-chip stimulated Brillouin scattering via surface acoustic waves," (2023), arXiv:2310.01707.
[28]P. Dainese, P. S. J. Russell, N. Joly, J. Knight, G. Wiederhecker, H. L. Fragnito, V. Laude, and A. Khelif, "Stimulated Brillouin scattering from multi-ghz-guided acoustic phonons in nanostructured photonic crystal fibres," Nature Physics **2**, 388–392 (2006).
[29]C. Wolff, R. Van Laer, M. J. Steel, B. J. Eggleton, and C. G. Poulton, "Brillouin resonance broadening due to structural variations in nanoscale waveguides," New Journal of Physics **18**, 025006 (2016).
[30]S. P. Smith, F. Zarinetchi, and S. Ezekiel, "Narrow-linewidth stimulated Brillouin fiber laser and applications," Opt. Lett. **16**, 393–395 (1991).
[31]A. Sebastian, I. V. Balakireva, S. Fresnel, S. Trebaol, and P. Besnard, "Relative intensity noise in a multi-Stokes Brillouin laser," Opt. Express **26**, 33700–33711 (2018).
[32]S. Gundavarapu, G. M. Brodnik, M. Puckett, T. Huffman, D. Bose, R. Behunin, J. Wu, T. Qiu, C. Pinho, N. Chauhan, J. Nohava, P. T. Rakich, K. D. Nelson, M. Salit, and D. J. Blumenthal, "Sub-Hertz fundamental linewidth photonic integrated Brillouin laser," Nature Photonics **13**, 60–67 (2019).
[33]G. Danion, M. Vallet, L. Frein, P. Szriftgiser, and M. Alouini, "Brillouin Assisted Optoelectronic Self-Narrowing of Laser Linewidth," IEEE Photonics Technology Letters **31**, 975–978 (2019).
[34]M. Deroh, E. Lucas, K. Hammani, G. Millot, and B. Kibler, "Stabilized single-frequency sub-kHz linewidth Brillouin fiber laser cavity operating at 1 µm," Appl. Opt. **62**, 8109–8114 (2023).
[35]G. P. Agrawal, *Nonlinear Fiber Optics 6th ed.* (Academic Press, 2019).
[36]K. Hu, I. V. Kabakova, T. F. S. Büttner, S. Lefrancois, D. D. Hudson, S. He, and B. J. Eggleton, "Low-threshold Brillouin laser at 2 µm based on suspended-core chalcogenide fiber," Optics letters **39**, 4651–4654 (2014).
[37]J. Kierzenka and L. F. Shampine, "A BVP solver based on residual control and the Maltab PSE," ACM Trans. Math. Softw. **27**, 299–316 (2001).
[38]L. Chen and X. Bao, "Analytical and numerical solutions for steady state stimulated Brillouin scattering in a single-mode fiber," Optics Communications **152**, 65–70 (1998).
[39]E. Lucas, M. Deroh, and B. Kibler, "Dynamic Interplay Between Kerr Combs and Brillouin Lasing in Fiber Cavities," Laser & Photonics Reviews **17**, 2300041 (2023).
[40]M. Dong and H. G. Winful, "Unified approach to cascaded stimulated Brillouin scattering and frequency-comb generation," Phys. Rev. A **93**, 043851 (2016).
[41]T. F. S. Büttner, I. V. Kabakova, D. D. Hudson, R. Pant, C. G. Poulton, A. C. Judge, and B. J. Eggleton, "Phase-locking and Pulse Generation in Multi-Frequency Brillouin Oscillator via Four Wave Mixing," Sci Rep **4**, 5032 (2014).